Research Square

Preprints are preliminary reports that have not undergone peer review.
They should not be considered conclusive, used to inform clinical practice,
or referenced by the media as validated information.

A Self-Powered Photoelectrochemical Sensor Based on an In2O3/Ag2S Heterojunction for Tetracycline Detection and Portable Applications

Junyu Li
Zhejiang A&F University
Haoyu Li
Zhejiang A&F University
Yujie Hao
Zhejiang A&F University
Jiawei Pu
Zhejiang A&F University
Linmei Ye
Wei Liu
liuwei@zafu.edu.cn

Zhejiang A&F University

Research Article

Keywords: Heterojunction-based, Photoelectrochemical (PEC) sensor, Tetracycline detection, Portable applications, Environmental monitoring

Posted Date: April 16th, 2026

DOI: https://doi.org/10.21203/rs.3.rs-9265811/v1

License: This work is licensed under a Creative Commons Attribution 4.0 International License.
Read Full License

Additional Declarations: No competing interests reported.

Version of Record: A version of this preprint was published at Microchimica Acta on June 5th, 2026. See the published version at https://doi.org/10.1007/s00604-026-08170-9.

Abstract

Tetracycline (TC) is a widely used broad-spectrum antibiotic that effectively inhibits a variety of bacteria. However, its extensive application has resulted in the release of residual TC into aquatic environments, where it has become a typical emerging contaminant that promotes bacterial resistance and disrupts ecological balance. In this study, a self-powered photoelectrochemical (PEC) sensor based on an In_2O_3/Ag_2S heterojunction was developed for the sensitive detection of tetracycline residues in water. In_2O_3 with excellent photoelectric properties was first synthesized via a reflux-heating method followed by calcination. Subsequently, an In_2O_3/Ag_2S heterojunction was successfully constructed through an in situ growth strategy, exhibiting a significantly enhanced photoelectric response and a strong, stable initial photocurrent. Under optimized conditions, the proposed sensor exhibited a linear detection range for tetracycline from 1 nM to 1 mM, with a detection limit as low as 0.4 nM. In addition, the sensor demonstrated good stability, rapid response, high selectivity, and excellent reproducibility. Furthermore, by integrating a microcontroller-based system, sensor portability was achieved, offering a promising approach for the development of portable photoelectrochemical sensing technologies.

1. Introduction

Antibiotics are secondary metabolites produced by microorganisms as well as higher plants and animals, and they exhibit anti-pathogenic activity. They exert their effects by inhibiting bacterial growth or inducing cell death through mechanisms such as suppression of cell wall synthesis, inhibition of protein synthesis, and interference with nucleic acid replication[1]. Tetracycline (TC), recognized as the first broad-spectrum antibiotic [2], has been extensively used in the treatment of respiratory infections, acne, and other diseases. However, owing to its widespread application and incomplete metabolism in organisms, TC is continuously released into the environment through livestock wastewater, medical effluents, and domestic sewage [3]. As a persistent aquatic pollutant, TC not only disrupts ecological balance but also poses a potential threat to public health security [4]. Therefore, the development of highly sensitive and rapid-response detection systems for tetracycline, along with the implementation of effective control strategies, is of critical importance.

To date, a variety of analytical methods have been developed for tetracycline (TC) detection. Specifically, high-performance liquid chromatography (HPLC) [5], and its hyphenated techniques offer high accuracy but require expensive columns and sophisticated pre-treatment. Colorimetric assays [6], and fluorescence spectroscopy [7], provide visual or sensitive detection, yet they are frequently susceptible to the inherent color or turbidity of environmental matrices.The chemiluminescence [8], and electrochemical techniques [9] while cost-effective, often suffer from high background noise due to the simultaneous excitation of capacitive currents. By contrast, photoelectrochemical (PEC) sensing technology has attracted increasing attention owing to its inherent advantages, such as high sensitivity, rapid response, operational simplicity, and low background interference, and has been widely applied to the detection of diverse environmental contaminants [10]. Nevertheless, a critical challenge in PEC sensing remains the development of photoactive materials with strong signal responses and long-term

photoelectrochemical stability. In this context, metal oxides have emerged as promising candidates because of their excellent chemical stability, resistance to photocorrosion, and versatile synthesis strategies. For example, Shinde et al. constructed a ZnO/MoS_2 heterojunction based on ZnO nanotube arrays, achieving enhanced PEC performance [11]. Similarly, Tao et al. developed a Pt_1–p–TiO_2photoanode with outstanding photoelectric properties using TiO_2 nanorod arrays [12]. These studies collectively highlight the broad application potential of metal oxide-based materials in PEC sensing.

In_2O_3, as an n-type semiconductor, plays an important role in photoelectric sensing and detection owing to its high electrical conductivity, excellent stability, and strong resistance to photodegradation. However, its wide bandgap and unfavorable valence band structure lead to limited visible-light absorption, thereby restricting its practical application potential [13–15]. In contrast, Ag_2S exhibits high photosensitivity, featuring a narrow bandgap of approximately 1 eV and strong absorption across the visible to near-infrared spectral region [16–18]. Moreover, when coupled with other semiconductors to form heterojunctions, Ag_2S can effectively promote the separation and transfer of photogenerated charge carriers, thereby significantly enhancing the photocatalytic and photoelectrochemical performance of composite materials [19]. Based on these considerations, a self-powered photoelectrochemical sensor based on an In_2O_3/Ag_2S heterojunction was successfully constructed via an in situ growth strategy and applied for the high-performance detection of tetracycline (TC). Experimental results demonstrate that the as-fabricated sensor exhibits high sensitivity, excellent selectivity, good stability, and satisfactory reproducibility, indicating its promising potential for practical applications.

2. Experimental Section

2.1. Reagents and Instruments

Tetracycline (TC), $In(NO_3)_3{\cdot}xH_2O$, terephthalic acid (PTA), $AgNO_3$, Na_2S, and ascorbic acid (AA) were purchased from Aladdin Chemical Co., Ltd. All chemicals were of analytical grade and used as received without further purification. All aqueous solutions were prepared using ultrapure water.

The morphology and microstructure of the samples were characterized by field-emission scanning electron microscopy (FESEM, Carl Zeiss Ultra Plus). X-ray photoelectron spectroscopy (XPS) was employed to investigate the elemental valence states and surface chemical compositions of the samples, using Mg Kα radiation on a PerkinElmer PHI 3056 spectrometer. X-ray diffraction (XRD, Bruker D8 Advance) was used to identify the crystal structures and phase compositions. Raman spectra were collected at room temperature using a confocal micro-Raman spectrometer (Hangzhou Pura Photoelectric Co., Ltd.) with a 532 nm laser as the excitation source. UV–Vis diffuse reflectance spectra (DRS) were recorded using a UV–Vis spectrophotometer (PerkinElmer Lambda 1050+).

2.2. Preparation of In_2O_3/Ag_2S/ITO

Hexagonal tubular In_2O_3 was derived from an indium-based metal–organic framework (MIL-68(In)). As illustrated in Fig. 1, the fabrication process of In_2O_3/ITO is described as follows. First, MIL-68(In) with a hexagonal prismatic morphology was synthesized via a solvothermal reflux method. Specifically, 0.2 mmol of $In(NO_3)_3 \cdot xH_2O$ and 0.4 mmol of terephthalic acid were dissolved in 30 mL of N,N-dimethylformamide (DMF) under continuous stirring for 30 min. The resulting solution was then heated in an oil bath at 120°C for 1 h. After completion of the reaction, the mixture was allowed to cool naturally to room temperature, and the resulting white precipitate was collected by centrifugation. The precipitate was washed several times with ethanol and DMF, followed by vacuum drying at 60°C. Subsequently, the dried powder was placed in a crucible and calcined in a tube furnace under an air atmosphere. The temperature was gradually increased to 600°C at a heating rate of 2°C min^{-1} and maintained for 2 h, yielding hexagonal tubular In_2O_3 [20].

Subsequently, 3 mg of In_2O_3 was dispersed in 1 mL of deionized water and ultrasonicated to obtain a homogeneous suspension. The resulting suspension was drop-cast onto an indium tin oxide (ITO) conductive glass substrate that had been sequentially cleaned with acetone, ethanol, and deionized water, and then allowed to dry naturally at room temperature.

Ag_2S was deposited onto the In_2O_3/ITO electrode via the successive ionic layer adsorption and reaction (SILAR) method. Briefly, the In_2O_3/ITO electrode was immersed in a 50 mM $AgNO_3$ solution for 4 min to allow the adsorption of Ag^+ ions. The electrode was then rinsed with ethanol for 1 min to remove excess Ag^+ ions from the In_2O_3 surface. Subsequently, the electrode was immersed in a 25 mM Na_2S solution, enabling S^{2-}ions to react with the adsorbed Ag^+ ions to form Ag_2S on the In_2O_3 surface. Finally, the electrode was immersed in methanol for 1 min to remove residual Ag_2S species [21]. This SILAR cycle was repeated multiple times to obtain the In_2O_3/Ag_2S/ITO electrode.

Figure 1. Schematic illustration of the fabrication process and photoelectrochemical testing of the In_2O_3/Ag_2S/ITO electrode.

2.3. Electrochemical Measurements

Electrochemical characterization of the In_2O_3/Ag_2S/ITO electrode was carried out using a standard three-electrode system on a CHI 660E electrochemical workstation (CH Instruments, Shanghai, China). A 0.1 M ascorbic acid (AA) solution (pH 7.4) served as the electrolyte. An Ag/AgCl electrode and a platinum wire were employed as the reference and counter electrodes, respectively. A 500 W Xe lamp (Solar-500 W) was used as the light source for photoelectrochemical (PEC) measurements. All experiments were conducted at room temperature. A custom-built programmable movable platform was utilized to control the light shutter, with the light source cycled on and off every 20 s. No external bias voltage was applied during the tests.

3. Results and Discussion

3.1. Material Characterization

The morphologies of the synthesized In_2O_3 and the In_2O_3/Ag_2S composite were examined using scanning electron microscopy (SEM). Figures 2A and 2B present micrographs of In_2O_3 at different magnifications, revealing that the material prepared via the solvothermal reflux-calcination method retained a hexagonal prismatic crystal structure similar to that of its MIL-68(In) precursor [22]. The individual prisms exhibited an approximate length of 5 μm and a cross-sectional radius of around 500 nm. In addition, several voids were observed on the surface, which are attributed to the decomposition of organic ligands during calcination [23].

Ag_2S was subsequently composited onto the In_2O_3 surface via an in-situ growth method. As shown in Figs. 2C and 2D, Ag_2S formed a uniform coating on the rod-like In_2O_3 framework. Energy-dispersive X-ray spectroscopy (EDS) elemental mapping of a selected area (Fig. 2E) confirmed the homogeneous distribution of Ag, In, O, and S elements (Fig. 2F–2I), providing further evidence of the uniform deposition of Ag_2S on the In_2O_3 surface.

Figure 2. SEM images of In_2O_3 (A, B) and In_2O_3/Ag_2S composites (C–E), along with EDS elemental mapping of Ag (F), In (G), O (H), and S (I).

The crystal structures of In_2O_3 and the In_2O_3/Ag_2S (Fig. 3A) composite were analyzed by X-ray diffraction (XRD). The diffraction peaks of In_2O_3 matched well with the standard JCPDS card (No. 88-2160) without any impurity peaks, indicating high crystallinity and phase purity. Upon incorporation of Ag_2S, additional characteristic diffraction peaks corresponding to monoclinic α-Ag_2S (JCPDS No. 14–0072) appeared in the XRD pattern. Peaks at 31.5°, 34.4°, and 36.8° were assigned to the (-121), (022), and (121) crystal planes, respectively, confirming the successful construction of the heterojunction [24, 25].

The surface composition and chemical states of the materials (Fig. 3B-F) were further examined by X-ray photoelectron spectroscopy (XPS). The survey spectrum confirmed the presence of characteristic signals for In, O, Ag, and S. In the high-resolution In 3d spectrum, binding energies at 443.96 eV and 451.49 eV were attributed to In^{3+} $3d_{5/2}$ and In^{3+} $3d_{3/2}$ respectively. The O 1s spectrum exhibited a peak at 528.95 eV, corresponding to lattice oxygen in In_2O_3 [26, 27]. In addition, the Ag 3d spectrum displayed peaks at 367.2 eV and 373.2 eV, assigned to Ag^+ $3d_{5/2}$ and Ag^+ $3d_{3/2}$ respectively. The S 2p spectrum showed binding energies at 160.8 eV and 162.0 eV, corresponding to S^{2-} $2p_{3/2}$ and S^{2-} $2p_{1/2}$. These results are consistent with previously reported XPS characteristics of metal sulfides [28, 29], further confirming the successful synthesis of the In_2O_3/Ag_2S composite.

Figure 3. Characterization of In_2O_3/Ag_2S: (A) XRD pattern, (B) XPS survey spectrum, and high-resolution XPS spectra of In 3d (C), O 1s (D), Ag 3d (E), and S 2p (F).

3.2 PEC Sensor for TC Detection

Raman scattering spectroscopy characterization (Fig. 4A) revealed that In_2O_3 exhibited two distinct peaks at 122 cm^{-1} and 460 cm^{-1}. After constructing the In_2O_3/Ag_2S heterojunction via the in-situ growth method, additional peaks appeared at 300 cm^{-1}. and 365 cm^{-1}., further confirming the successful formation of the heterojunction [30]. Notably, the In_2O_3 peak at 122 cm^{-1}. exhibited a slight redshift, primarily attributed to macroscopic tensile stress induced by lattice thermal expansion, which causes lattice expansion and softens the vibrational mode. In contrast, the blueshift observed at 460 cm^{-1}. resulted from strong chemical bonding at the interface, which stiffened the high-frequency vibrational mode and shifted the peak to a higher wavenumber.

To investigate the band structure of the heterojunction and the electron-hole transfer mechanism of the sensor, UV-Vis diffuse reflectance spectroscopy was used to construct a Tauc plot (Fig. 4B). The band gaps of In_2O_3 and Ag_2S were calculated as follows [31]:

1. Kubelka-Munk (K-M) function conversion:

The diffuse reflectance is converted to the Kubelka-Munk function F(R∞) using the Eq. 1:

$$F\left(R\right) = \frac{\left(1-R\right)^2}{R}$$

1

In this formula, R is the reflectance, typically measured using a $BaSO_4$ white plate as the baseline. The sample was uniformly coated on $BaSO_4$ to obtain the reflectance. The K-M function standardizes the characterization of the material's light absorption capability.

1. Application of the Tauc relation:

$$\left(F\left(\,R\right)\cdot\ h\nu\,\right)^{1/n} = B(h\nu\ - Eg)$$

2

In this formula, h is Planck's constant, v is the frequency of light, Eg is the bandgap energy, and n is a constant related to the nature of the semiconductor: n = 2 for indirect bandgap semiconductors and n = 1/2 for direct bandgap semiconductors. For In_2O_3 and Ag_2S, n was set to 2 and 1/2, respectively. The Tauc plot (Fig. 4B) was generated by plotting $(F(R)\cdot hv)^{1/n}$ on the ordinate versus hv on the abscissa.

1. Calculation of bandgap (E_g):

Linear fitting was performed in the appropriate region of the Tauc plot using the tangent tool (y_1 = -122.40612 + 35.00393x; y_2 = -2.97727 + 2.38203x) intercept on the horizontal axis (hv), provided the bandgap energies of In_2O_3 and Ag_2S, calculated as 3.49 eV and 1.24 eV, respectively [32].

Figure 4C illustrates the electron-hole transfer mechanism of the PEC sensor. Under xenon lamp irradiation, both In_2O_3 and Ag_2S generate electron-hole pairs. Due to the favorable band alignment, electrons from the conduction band of Ag_2S migrate to the conduction band of In_2O_3 and undergo reduction reactions at the working electrode interface($OH^{\cdot} + e^{-} \rightarrow OH^{-}$). Simultaneously, holes migrate in the opposite direction and are efficiently captured by ascorbic acid (AA) as an electron donor. This process significantly suppresses electron-hole recombination, thereby enhancing the photocurrent signal [33].

Figure 4. Characterization and working mechanism of the In_2O_3/Ag_2S/ITO sensor: Raman spectra of In_2O_3 and In_2O_3/Ag_2S (A), Tauc plots for bandgap estimation (B), and schematic illustration of the electron-hole transfer process (C).

To systematically evaluate the enhancement effect of the heterojunction structure on the photoelectric performance, chronoamperometry measurements were carried out under zero bias potential using a three-electrode system on ITO electrodes modified with In_2O_3 and In_2O_3/Ag_2S [34]. As shown in Fig. 5A, in a PBS buffer solution (pH 7.4, containing 0.1 M AA), the photocurrent response of the In_2O_3/Ag_2S composite reached 150–180 μA, significantly higher than that of the pure In_2O_3 electrode. This improvement is primarily attributed to the heterojunction structure, which effectively promotes photogenerated carrier separation and transport. The built-in electric field at the interface not only accelerates electron-hole pair separation and prolongs carrier lifetime but also provides an efficient transport pathway due to the well-aligned band structure, thereby substantially enhancing photoelectric conversion efficiency [35–37].

The effect of different Ag_2S growth cycles on photoelectric performance was further investigated (Fig. 5B). As the number of cycles increased, Ag_2S achieved more uniform and complete coverage on the In_2O_3 surface, enlarging the interfacial contact area and facilitating carrier separation and collection. However, when the number of cycles exceeded nine, excessive particle agglomeration reduced the effective contact area and introduced interfacial defects, which weakened the synergistic electron transport effect [38, 39].

Under optimal conditions, continuous on-off light cycling over 20 cycles (Fig. 5C) demonstrated that the sensor's photocurrent remained stable with negligible attenuation. The calculated photocurrent loss rate was only 3%, indicating that the In_2O_3/Ag_2S heterojunction sensor exhibits excellent photostability and resistance to photodegradation.

To evaluate the detection performance of the constructed In_2O_3/Ag_2S/ITO sensor, photocurrent responses to tetracycline (TC) standard solutions of varying concentrations were measured [40, 41]. As shown in Fig. 6A, TC concentrations ranging from 1 nM to 1 mM were tested. The photocurrent response (I) exhibited a clear linear relationship with TC concentration across this range (Fig. 6B). The first linear segment, covering 1 nM to 5 μM, was described by the regression equation I (μA) = − 6.861 lgC (nmol/L)

+ 136.246 with a correlation coefficient of R_1^2 = 0.992. The second segment, spanning 5 μM to 1 mM, followed I (μA) = − 21.499 lgC (nmol/L) + 192.839 with R_2^2 = 0.982.

A decreasing trend in photocurrent was observed with increasing TC concentration. This behavior can be primarily attributed to the progressive capture of photogenerated holes by TC molecules in the electrolyte, which accelerates electron-hole recombination and reduces the effective charge contributing to the current, thereby lowering the photocurrent. The two-segment linear response is attributed to the availability of high-activity sites on the photoelectrode surface: at low concentrations, these sites participate preferentially, resulting in higher sensitivity in the first segment. As the concentration increases beyond a threshold, the high-activity sites become saturated, and the reaction shifts to lower-activity sites, reducing sensitivity in the second segment and producing different slopes for the two linear regions. Based on the regression equation of the second segment, the limit of detection (LOD) of the sensor was determined to be 0.4 nM according to the IUPAC-recommended method[42].

To evaluate the detection performance of the constructed In_2O_3/Ag_2S/ITO sensor, photocurrent responses to tetracycline (TC) standard solutions of varying concentrations were measured [40, 41]. As shown in Fig. 6A, TC concentrations ranging from 1 nM to 1 mM were tested. The photocurrent response (I) exhibited a clear linear relationship with TC concentration across this range (Fig. 6B). The first linear segment, covering 1 nM to 5 μM, was described by the regression equation I (μA) = − 6.861 lgC (nmol/L) + 136.246 with a correlation coefficient of R_1^2 = 0.992. The second segment, spanning 5 μM to 1 mM, followed I (μA) = − 21.499 lgC (nmol/L) + 192.839 with R_2^2 = 0.982.

A decreasing trend in photocurrent was observed with increasing TC concentration. This behavior can be primarily attributed to the progressive capture of photogenerated holes by TC molecules in the electrolyte, which accelerates electron-hole recombination and reduces the effective charge contributing to the current, thereby lowering the photocurrent. The two-segment linear response is attributed to the availability of high-activity sites on the photoelectrode surface: at low concentrations, these sites participate preferentially, resulting in higher sensitivity in the first segment. As the concentration increases beyond a threshold, the high-activity sites become saturated, and the reaction shifts to lower-activity sites, reducing sensitivity in the second segment and producing different slopes for the two linear regions. Based on the regression equation of the second segment, the limit of detection (LOD) of the sensor was determined to be 0.4 nM according to the IUPAC-recommended method[42].

Figure 6. Photoelectrochemical detection of tetracycline using the In_2O_3/Ag_2S/ITO sensor: (A) photocurrent responses at different TC concentrations (1nM − 1mM) and (B) the corresponding linear calibration curves3.3. Selectivity, Reproducibility, and Stability of the PEC Sensor

The analytical performance of the In_2O_3/Ag_2S/ITO sensor was systematically evaluated in terms of selectivity, reproducibility, and stability. In selectivity tests, for selectivity tests, water samples from the Oujiang River in Qingtian County, Lishui City, Zhejiang Province were collected and used as the testing

matrix, eight common interfering species (K^+, Cl^-, Na+, Ca^{2+}, SO_4^{2-}, PO_4^{3-}, bovine serum albumin, and glucose) were examined. Even when the concentration of interferents (5 mM) was ten times higher than that of tetracycline (50 μM), the photocurrent response induced by tetracycline remained significantly greater than that caused by any of the interfering species (Fig. 7A), demonstrating the high specificity of the sensor. This selectivity is primarily attributed to the specific interaction between the heterojunction surface and tetracycline molecules. Reproducibility was assessed using seven independently fabricated sensors under identical conditions, yielding a relative standard deviation (RSD) of 3.73% (Fig. 7B), which indicates the reliability of the fabrication process. Stability tests showed that the photocurrent response of the same sensor retained more than 95% of its initial value after storage at room temperature for 7 days (Fig. 7C), confirming excellent long-term operational stability.

Figure 7. Analytical performance of the In_2O_3/Ag_2S/ITO sensor: (A) selectivity against common interfering species, (B) reproducibility at a tetracycline concentration of 5 μM, and (C) photocurrent stability over seven days.

3.4 Portable PEC Sensor

To explore the practical feasibility of the developed photosensor, a preliminary attempt at portable detection was conducted using a custom-built, MCU-based device (Fig. 8A) [43]. This prototype system serves as a proof-of-concept for transitioning laboratory research toward on-site environmental analysis. Experimental results indicate that, despite the precision limitations of the portable hardware which lead to a narrower linear detection range compared to laboratory equipment (Fig. 8B), the In_2O_3/Ag_2S sensor maintains reliable signal stability and consistent response trends. This limitation primarily arises from the relatively small voltage fluctuations induced by low TC concentrations relative to the background signal. The linear regression for this portable configuration, expressed as y(mV) = 85.061-13.459lgC(μmol/L) (R^2 = 0.9746), alongside a calculated LOD of 0.536 μmol/L, demonstrates that the heterojunction possesses sufficient analytical performance for rapid field screening. While laboratory instruments remain the gold standard for high-sensitivity quantification, this portable attempt highlights a promising direction for developing low-cost, decentralized sensing platforms for real-time monitoring of antibiotic contaminants.

Figure 8. Portable PEC sensor: (A) Photocurrent responses of the device at different tetracycline concentrations (1, 5, 10, 50 μM; 0.1, 0.5, 1 mM). (B) Corresponding photocurrent response curves. (C) Linear calibration curve for tetracycline detection.

A comparison of the constructed sensor (in both standard and portable configurations) with previously reported tetracycline sensors is summarized in Table 1. The results demonstrate that the developed sensor achieves both a wide detection range and a low detection limit. Its performance in the portable system further highlights its potential for practical, on-site applications.

Table 1
Comparison of the developed In_2O_3/Ag_2S PEC sensor with previously reported tetracycline sensors:

Materials	Test item	Linear	LOD	References
g-C_3N_4/$BiVO_4$	**Tetracycline**	**5 -200 nM**	**1.6 nM**	[44]
$AgInS_2$ quantum dots	**Tetracycline**	**1.3 nM-100 μM**	**0.6 nM**	[45]
Cu_2MoS_4@Ti_3C_2Tx	**Tetracycline**	**5 -300 nM**	**1.24 nM**	[46]
Ti_3O/R-TiO_2	**Tetracycline**	**3 -300 μM**	**0.039μM**	[47]
In_2O_3/Ag_2S	**Tetracycline**	**1 nM-1 mM**	**0.4 nM**	**This Work**
In_2O_3/Ag_2S Mobile	**Tetracycline**	**1μM-1mM**	**0.536 μM**	**This Work**

Conclusion

In this work, a self-powered photoelectrochemical (PEC) sensor based on an In_2O_3/Ag_2S heterojunction, prepared via an in-situ growth method, was successfully developed for the detection of tetracycline in aqueous environments. The fabricated PEC sensor offers several advantages, including low fabrication cost, simple operation, and excellent photoelectric performance. Experimental results demonstrated a wide detection range from 1 nM to 1 mM, with a detection limit as low as 0.4 nM. In addition, the sensor exhibited high selectivity, stability, and reproducibility. By integrating a microcontroller unit (MCU), a preliminary portable PEC device was constructed, achieving a detection range of 1 μM to 1 mM with a calculated detection limit of 0.536 μM. This work not only advances PEC-based detection of water pollutants but also provides a new strategy for tetracycline monitoring and promotes the development of portable PEC sensing technology.

Declarations

Author Contribution

Junyu Li : Data curation, Writing- Original draft. Haoyu Li : Data curation. Yujie Hao : Data curation, Investigation. Jiawei Pu : Investigation. Linmei Ye : Writing- Reviewing and editing, Data curation, Investigation. Wei Liu : Writing- Reviewing and editing, Supervision.

Acknowledgement

This work was supported by Zhejiang Provincial Academy Cooperation Forestry Science and Technology Project (2023SY14), the Funds of the Natural Science Foundation of Hangzhou (Grant No. 2024SZRYBC130002), Natural Science Foundation of Zhejiang Province (Grant No. LQN25C160004,

LTGC23C160002), the Scientific Research and Developed Fund of Zhejiang A&F University (Grant No2022LFR042, 2022LFR107).

CRediT authorship contribution statement

Junyu Li: Data curation, Writing- Original draft. **Haoyu Li**: Data curation. **Yujie Hao**: Data curation, Investigation. **Jiawei Pu**: Investigation. **Linmei Ye**: Writing- Reviewing and editing, Data curation, Investigation. **Wei Liu**: Writing- Reviewing and editing, Supervision.

References

1. Scott GI, Porter DE, Norman RS, Scott CH, Uyaguari-Diaz MI, Maruya KA, Weisberg SB, Fulton MH, Wirth EF, Moore J, Pennington PL, Schlenk D, Cobb GP, Denslow ND (2016) Antibiotics as CECs: An Overview of the Hazards Posed by Antibiotics and Antibiotic Resistance. Front Mar Sci. https://doi.org/10.3389/fmars.2016.00024
2. Khalid R, Din MI, Hussain Z (2024) A critical overview on impact of different nano-catalytic assemblies for photodegradation of tetracycline. Rev Chem Eng. https://doi.org/10.1515/revce-2023-0029
3. Amangelsin Y, Semenova Y, Dadar M, Aljofan M, Bjørklund G (2023) The Impact of Tetracycline Pollution on the Aquatic Environment and Removal Strategies, Antibiotics https://doi.org/10.3390/antibiotics12030440
4. Tian L, Xu X, Zhang Z, Ding Y, Zhang K, Zhi S (2023) A Comprehensive Contamination Investigation of Bohai Bay Seawater: Antibiotics Occurrence, Distribution, Ecological Risks and Their Interactive Factors. Int J Environ Res Public Health. https://doi.org/10.3390/ijerph20021599
5. Wei YH, Li XY, Gao J, Liu JJ, Yuan D, Yin BC, Wang J (2018) Size-dependent modulation of CoOOH nanoflakes light scattering for rapid and selective detection of tetracycline in milk. J Anal Test. https://doi.org/10.1007/s41664-018-0080-6
6. Chang Y, He R, Wei Y, Wang L (2023) Polyethyleneimine-Sulfur Quantum Dot Composites for Dual-Channel Detection of Tetracycline by Colorimetric and Fluorescence Sensing. ACS Appl Nano Mater. https://doi.org/10.1021/acsanm.3c00506
7. Chen X, Lin J, Zhuang Y, Huang S, Chen J, Han Z (2022) Dual-mode turn-on ratiometric fluorescence sensor based on carbon dots and CuInS2/ZnS quantum dots for detection of chlorotetracycline. Spectrochim Acta Part A Mol Biomol Spectrosc. https://doi.org/10.1016/j.saa.2021.120851
8. Wang Y, He T, Ma L, Wen K (2025) Homogeneous chemiluminescence assay based on TetR allosteric effect for rapid detection of tetracyclines residues in milk. J Food Compos Anal. https://doi.org/10.1016/j.jfca.2025.108320
9. Dong W, Wen H, Du X, Li L, Li Z (2022) Electrochemical sensing of tetracycline based on Au NPs@MoS2/Ch hybrid structures. J Electroanal Chem. https://doi.org/10.1016/j.jelechem.2022.116807

10. Mao Y, Liu X, Bao Y, Niu L (2023) Recent Advances in Photoelectrochemical Sensors for Analysis of Toxins and Abused Drugs in the Environment, Chemosensors https://doi.org/10.3390/chemosensors11070412
11. Shinde P, Hase Y, Doiphode V, Bade BR, Kale D, Rahane S, Thombare J, Borkar D, Rondiya SR, Prasad M, Patole SP, Jadkar SR (2025) Morphology-Dependent ZnO/MoS2 Heterostructures for Enhanced Photoelectrochemical Water Splitting. ACS Appl Energy Mater. https://doi.org/10.1021/acsaem.4c02450
12. Tao Y, Ding J, Teng Z, Xu Q, Ou W, Sun H, Li S, Yu L, Li G, Liu B, Su C (2025) Single-Pt-Atom-Decorated TiO2 Nanorod Arrays for Photoelectrochemical C–H Chlorination. J Am Chem Soc. https://doi.org/10.1021/jacs.5c02551
13. Yan P, Huang J, Wu G, Zhang Y, Mo Z, Xu K, Ling M, Dong S, Xu L, Li H (2025) Construction of a In2O3/ultrathin g-C3N4 S-scheme heterojunction for sensitive photoelectrochemical aptasensing of diazinon. J Colloid Interface Sci 679:653–661. https://doi.org/10.1016/j.jcis.2024.10.016
14. Zhang N, Gao X, Guan H, Sun S, Liu J, Shao Z, Gao Q, Zhang Y, Sun R, Yang G, Gao F, Feng W (2023) Three-dimensional porous In2O3 arrays for self-powered transparent solar-blind photodetectors with high responsivity and excellent spectral selectivity. Nano Res 17(5):4471–4477. https://doi.org/10.1007/s12274-023-6370-y
15. Zhou Y, Sun R, Li H, Liu X, Song C, Wang D (2024) Design and application of hierarchical α-Fe2O3/In2O3 heterojunction photoanode for enhanced photoelectrochemical water oxidation. Int J Hydrog Energy 83:236–245. https://doi.org/10.1016/j.ijhydene.2024.08.065
16. Li M, Song Z, Li S, Khan MU, Wang Y, Xu Y, Wang S, Kong L, Chen Z, Sang F (2025) In situ Ag2S quantum dot-sensitized BiOI/Bi2O3 heterojunction: A label-free photoelectrochemical aptasensor for patulin detection, Talanta https://doi.org/10.1016/j.talanta.2025.128704
17. Wang H, Zhang Y, Zhang S, Fan D, Ren X, Kuang X, Wu D, Ma H, Liu X, Wei Q (2025) A high-throughput photoelectrochemical immunosensor array for light-addressing detection of Tau based on a competitive inhibition strategy between Ag2S@ZnO and Au@CeO2. Sens Actuators B. https://doi.org/10.1016/j.snb.2025.137429
18. Zhong Z, Ding L, Man Z, Zeng Y, Pan B, Zhu J-J, Zhang M, Cheng F (2024) Versatile Metal–Organic Framework Incorporating Ag2S for Constructing a Photoelectrochemical Immunosensor for Two Breast Cancer Markers. Anal Chem. https://doi.org/10.1021/acs.analchem.4c02091
19. Han Z, Song Y, Jia Y, Wang Y, Shi J, Liu X, Yu L, Li Z, Cheng Y, Zhang H, Jiang HY (2025) Classification and Characterization Methods for Heterojunctions. Adv Mater Interfaces. https://doi.org/10.1002/admi.202500191
20. Chen Q, Xue H, Lin Y, Chen L, Huang C, Zhao R, Ge H, Qiu B, Zhu J, Xu X (2024) Metal organic framework derived tubular-like indium trioxide to construct photoelectrochemical sensor for detecting carcinoembryonic antigen. Microchem J 202. https://doi.org/10.1016/j.microc.2024.110759

21. Chen Y-C, Kuo H-T, Lu Y-H, Hsu Y-K (2024) Improving Photoelectrochemical Activity of a Silver Sulfide-Based Photoelectrode by Bismuth Doping for Hydrogen Evolution from Industrial Waste Water. ACS Appl Energy Mater 7(11):4761–4767. https://doi.org/10.1021/acsaem.4c00447
22. Xu H, Chen H, Chen S, Wang K, Wang X (2021) Fabrication of In2O3/In2S3 heterostructures for enhanced photoelectrochemical performance. Int J Hydrog Energy 46(64):32445–32454. https://doi.org/10.1016/j.ijhydene.2021.07.085
23. Wu T, Feng J, Zhang S, Liu L, Ren X, Fan D, Kuang X, Sun X, Wei Q, Ju H (2020) A self-powered photoanode-supported photoelectrochemical immunosensor for CYFRA 21 – 1 detection based on In2O3/In2S3/CdIn2S4 heterojunction. Biosens Bioelectron 169. https://doi.org/10.1016/j.bios.2020.112580
24. Shi B, Qi Y, Tian L (2020) Fabrication of Ag2S quantum dots sensitized CdSe photoelectrodes and its photoelectric performance. Mater Chem Phys. https://doi.org/10.1016/j.matchemphys.2019.122177
25. Yadav J, Raturi P, Yadav S, Singh JP (2021) Zig-zag Ag2S nanostructures for superior optical absorption and photoelectrochemical water splitting performance. Renewable Energy. https://doi.org/10.1016/j.renene.2021.08.027
26. Wang Y, Zhu L, Liu Y, Vovk EI, Lang J, Zhou Z, Gao P, Li S, Yang Y (2023) Understanding surface structures of In2O3 catalysts during CO2 hydrogenation reaction using time-resolved IR, XPS with in situ treatment, and DFT calculations. Appl Surf Sci. https://doi.org/10.1016/j.apsusc.2023.157534
27. Wissink T, Rollier FA, Muravev V, Heinrichs JMJJ, van de Poll RCJ, Zhu J, Anastasiadou D, Kosinov N, Figueiredo MC, Hensen EJM (2024) Ce Promotion of In2O3 for Electrochemical Reduction of CO2 to Formate. ACS Catal. https://doi.org/10.1021/acscatal.4c02619
28. Chang C-J, Tsai Z-T, Lin K-S, Nian Y-H (2023) Enhanced photocatalytic H2 production of flower-like MoS2@Ag2S photocatalysts with matched band structures. J Photochem Photobiol A. https://doi.org/10.1016/j.jphotochem.2023.115027
29. Liu L, Ga L, Ai J (2024) Selective detection of Fe3 + by Ag2S QDs and construction of the IMPLICATION gate, Sensing and Bio. https://doi.org/10.1016/j.sbsr.2024.100624. -Sensing Research
30. Zhao N, Chang X, Liu X, Li J, Zheng W, Zhang J (2025) Probing the Structural Dynamics of In2O3 Using in Situ Raman Spectroscopy: Bridging Material Dynamics and Sensor Functionality. Angew Chem Int Ed. https://doi.org/10.1002/anie.202512808
31. Murphy A (2007) Band-gap determination from diffuse reflectance measurements of semiconductor films, and application to photoelectrochemical water-splitting. Sol Energy Mater Sol Cells. https://doi.org/10.1016/j.solmat.2007.05.005
32. Scanlon DO, Regoutz A, Egdell RG, Morgan DJ, Watson GW (2013) Band gap engineering of In2O3 by alloying with Tl2O3. Appl Phys Lett. https://doi.org/10.1063/1.4860986
33. Shi B, Chen B, Yan X, Cao H, Sun H, Wang D, Bi C, Wang C, Wang Y, Dai C, Liu W (2024) One-pot synthesis of stable and fast Bi2O2S/Bi2O3 heterojunction self-powered photoelectrochemical

sensors for sensitive detection of tetracycline. Mater Design 239. https://doi.org/10.1016/j.matdes.2024.112781

34. Wu H, Xu J, Zhao H, Shi B, Wan Y, Sun H, Wang D, Bi C, Wang C, Liu W (2025) One-step preparation of TiO2/PPy composite photoelectrochemical sensors and sensitive detection of TBZ and thiram. Chin J Phys. https://doi.org/10.1016/j.cjph.2025.08.039
35. Ji M-H, Chen Y-X, Chen R, Li K-X, Zhao H-P, Shi H-Y, Wang H-L, Jiang X, Lu C-Z (2023) A novel α-Fe2O3 photoanode with multilayered In2O3/Co–Mn nanostructure for efficient photoelectrochemical water splitting. Int J Hydrog Energy. https://doi.org/10.1016/j.ijhydene.2023.08.061
36. Li C, Wang M, Lei Y, Luo L, Wang Y, Du B, Deng Y, Tang Z, Chen J (2022) Photoelectrochemical Behavior of Simple Synthesized Cl-GQDs/In2O3. J Electrochem Soc. https://doi.org/10.1149/1945-7111/aca99d
37. Zhu X, Huang Q, Sun X, Hao Y, Wang H, Wu D, Ma H, Ju H, Wei Q (2023) Perylene tetracarboxylic acid (PTA)-based type II heterojunction sensing platform for signal-on photoelectrochemical detection of CEA. Sens Actuators B. https://doi.org/10.1016/j.snb.2023.134544
38. Li S, Li M, Zhao Z, Khan MU, Liu S, Kong L, Chen Z (2025) A photoelectrochemical aptasensor based on in-situ grown Ag2S quantum dot-sensitized Bi2MoO6/BiOBr heterojunction for α-lactalbumin detection. J Food Compos Anal. https://doi.org/10.1016/j.jfca.2025.108319
39. Zhao L, Chen H, Zhou J, Li P, Zhao W, Zhu X, Zhang Y, Liu M (2024) Alkaline Phosphatase-Decorated Au Nanoparticles Immobilized on Bi2S3 Particles Combined with Ag2S Quantum Dots as a Photoelectrochemical Sensing Platform for Alkaline Phosphatase Activity and Fluoride Ions. ACS Appl Nano Mater. https://doi.org/10.1021/acsanm.3c05917
40. Wang X, Cao Z, Shi B, Zhao A, Dai J, Wu S-T, Wang D, Liu W (2025) Machine learning-assisted photoelectrochemical/fluorescence dual-mode sensor for ultra-sensitive glyphosate detection. Chem Eng J. https://doi.org/10.1016/j.cej.2025.170337
41. Xiao Z, Chen Y, Zhang Y (2025) Self-powered portable photoelectrochemical sensor based on dual-photoelectrode for microplastics detection. Environ Res. https://doi.org/10.1016/j.envres.2025.121084
42. Cao H, Geng K, Yan X, Qiu H, Lin S, Dai C, Liu W, Wang Y (2023) Photoelectrochemical sensor based on Bi2(Te1-xSex)3 for the sensitive detection of the tetracycline hydrochloride. Mater Design. https://doi.org/10.1016/j.matdes.2023.112219
43. Wang X, Cao H, Cao Z, Ma X, Yin Z, Shi B, Dai C, Wang Y (2025) Enhanced portable photoelectrochemical strategy for oxalic acid detection: Using surface plasmonic resonance effect-activated Bi2Te2.85Se0.15 photoanode. Sens Actuators B. https://doi.org/10.1016/j.snb.2025.138036
44. Zhao Z, Wu Z, Lin X, Han F, Liang Z, Huang L, Dai M, Han D, Han L, Niu L (2022) A label-free PEC aptasensor platform based on g-C3N4/BiVO4 heterojunction for tetracycline detection in food analysis. Food Chem. https://doi.org/10.1016/j.foodchem.2022.134258

45. Guo M, Gu X, Yang B, He L, Yang J, Yan Y (2022) Highly sensitive detection for tetracycline residues in water based on its decreasing effect on photocurrent of AgInS2 quantum dots. J Environ Chem Eng. https://doi.org/10.1016/j.jece.2022.107714
46. Xu Y, Chen L, Guo X, Zhang J, Guo X, He Z, Zhang J, Han D (2025) Highly sensitive label-free photoelectrochemical aptasensor based on Cu2MoS4@Ti3C2Tx MXene heterojunction for tetracycline detection in milk. Microchim Acta 192(3). https://doi.org/10.1007/s00604-025-07016-0
47. Huang G, Si H, Zou L, Zhang H, Liao J, Lin S (2023) Phase Modulation of Ti3O/R-TiO2 Nanocomposites for the Self-Powered Photoelectrochemical Sensing of Tetracycline. ACS Appl Nano Mater. https://doi.org/10.1021/acsanm.3c04849

Figures

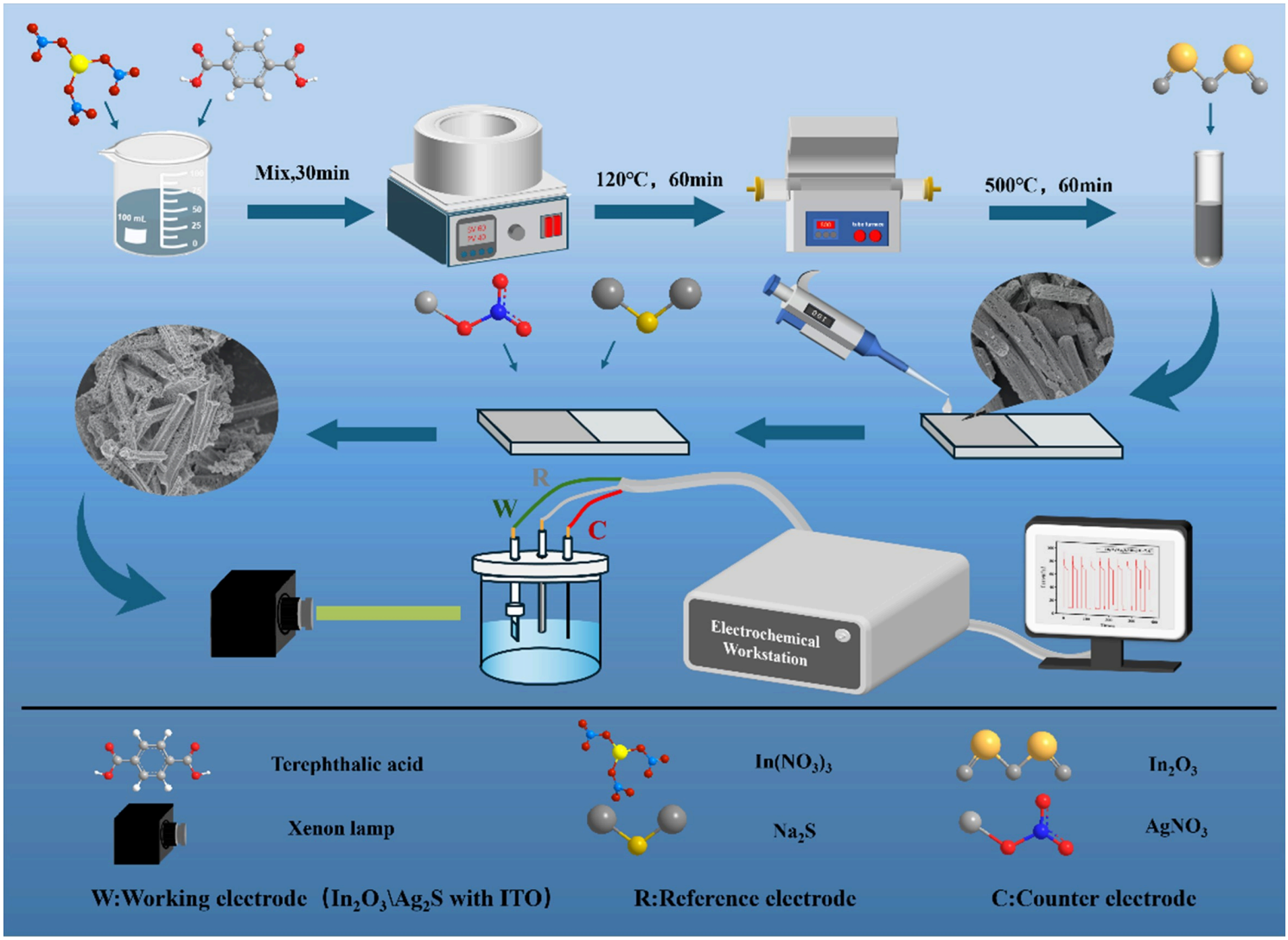


Figure 1

Schematic illustration of the fabrication process and photoelectrochemical testing of the In_2O_3/Ag_2S/ITO electrode.

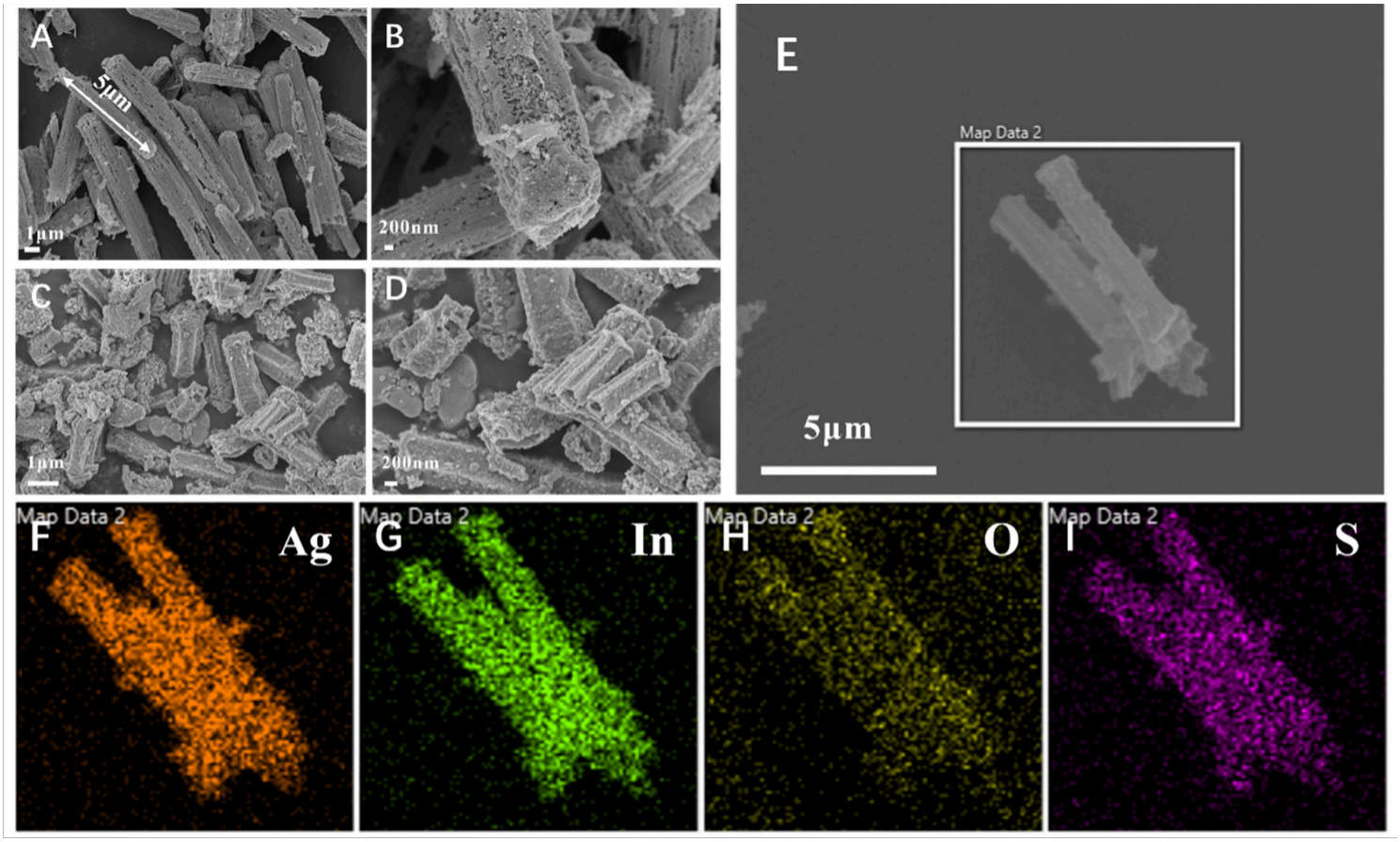


Figure 2

SEM images of In_2O_3 (A, B) and In_2O_3/Ag_2S composites (C–E), along with EDS elemental mapping of Ag (F), In (G), O (H), and S (I).

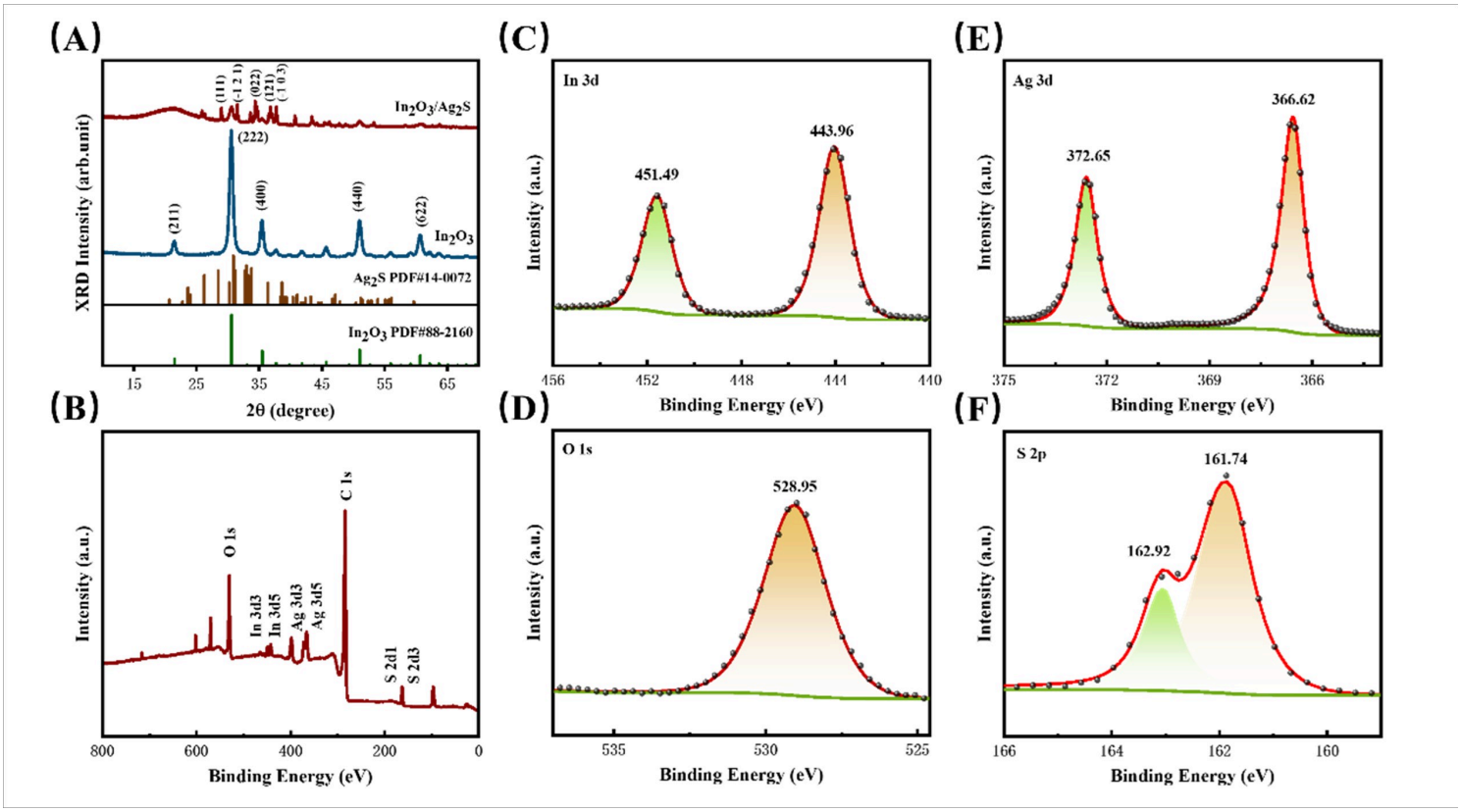


Figure 3

Characterization of In_2O_3/Ag_2S: (A) XRD pattern, (B) XPS survey spectrum, and high-resolution XPS spectra of In 3d (C), O 1s (D), Ag 3d (E), and S 2p (F).

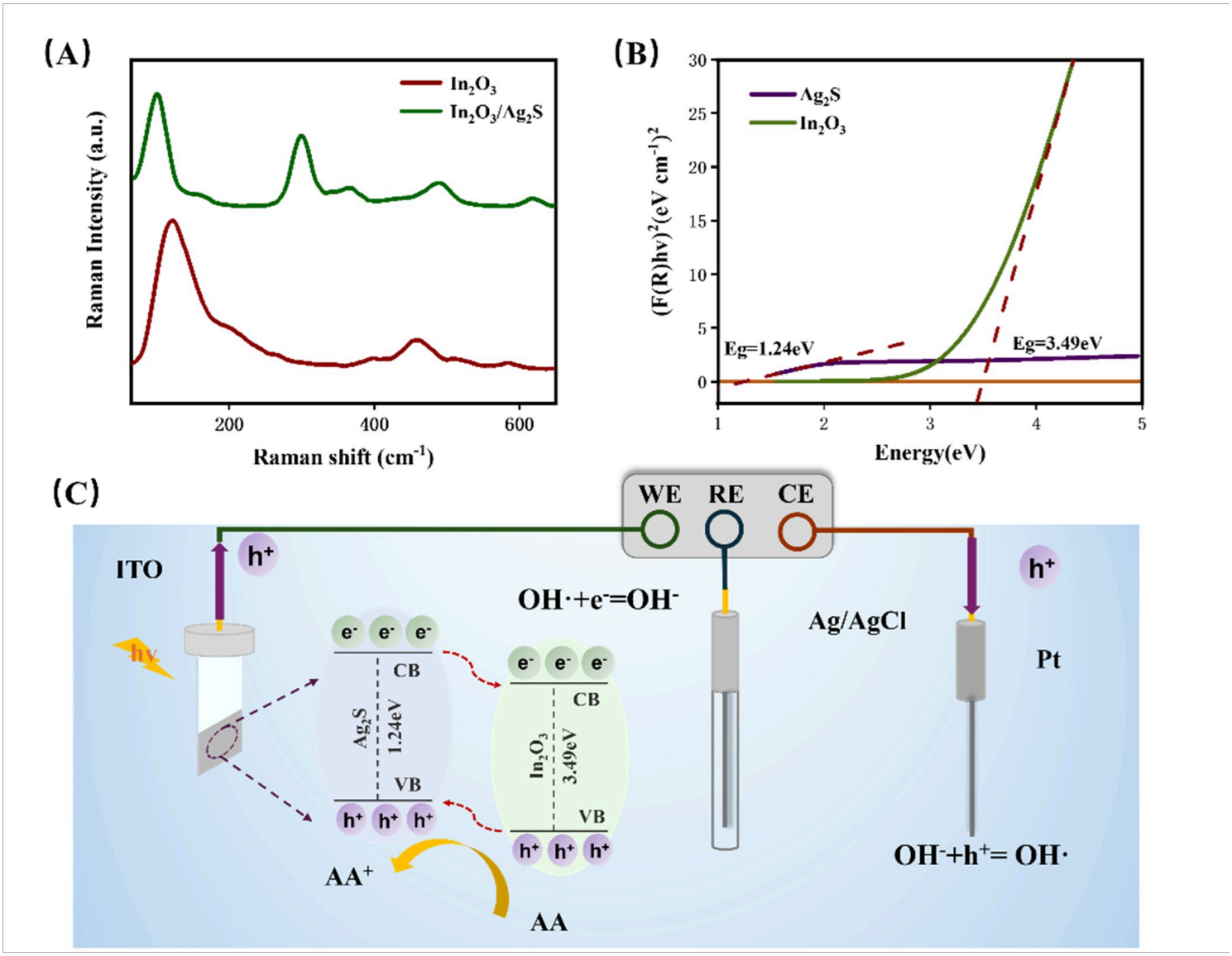


Figure 4

Characterization and working mechanism of the In_2O_3/Ag_2S/ITO sensor: Raman spectra of In_2O_3 and In_2O_3/Ag_2S (A), Tauc plots for bandgap estimation (B), and schematic illustration of the electron-hole transfer process (C).

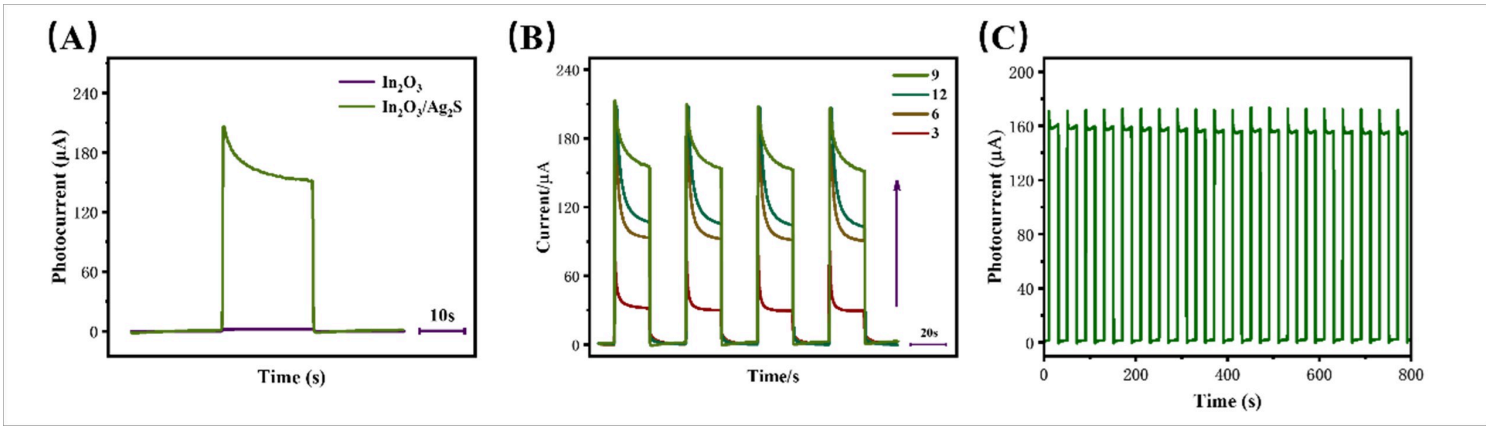


Figure 5

Photoelectrochemical performance of the In^2O^3/Ag^2S/ITO sensor: comparison of photocurrent responses between In_2O_3 and In_2O_3/Ag_2S (A), effect of different Ag_2S growth cycles on photocurrent (B), and photocurrent stability under continuous light cycling (C).

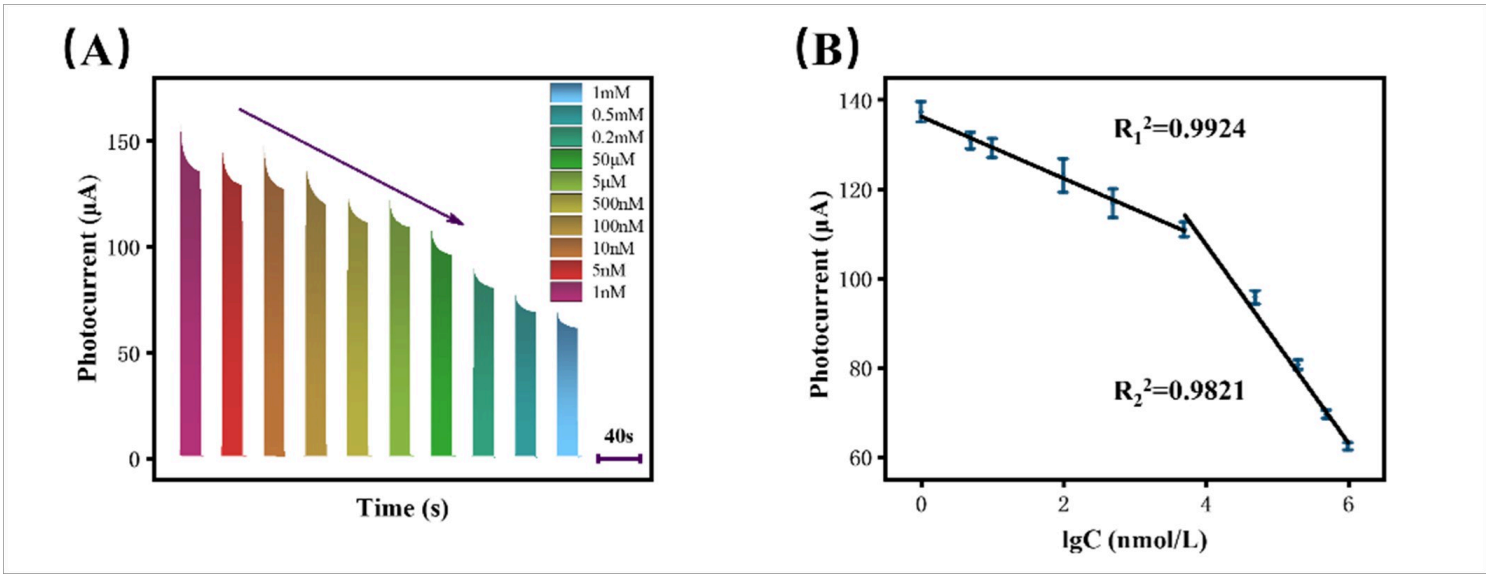


Figure 6

Photoelectrochemical detection of tetracycline using the In_2O_3/Ag_2S/ITO sensor: (A) photocurrent responses at different TC concentrations (1nM –1mM) and (B) the corresponding linear calibration curves3.3. Selectivity, Reproducibility, and Stability of the PEC Sensor

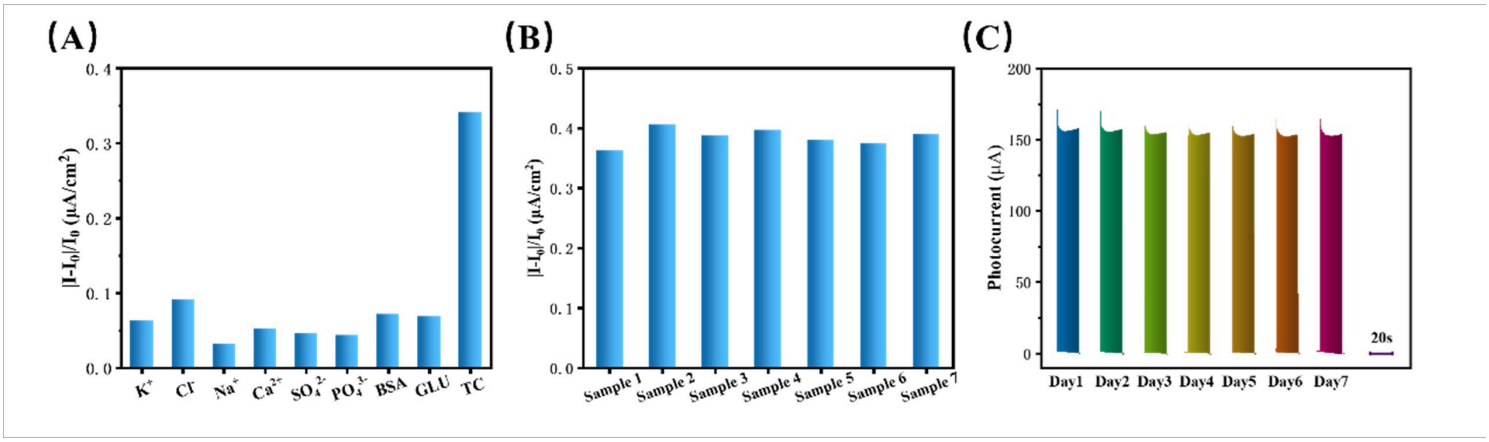


Figure 7

Analytical performance of the In_2O_3/Ag_2S/ITO sensor: (A) selectivity against common interfering species, (B) reproducibility at a tetracycline concentration of 5 μM, and (C) photocurrent stability over seven days.

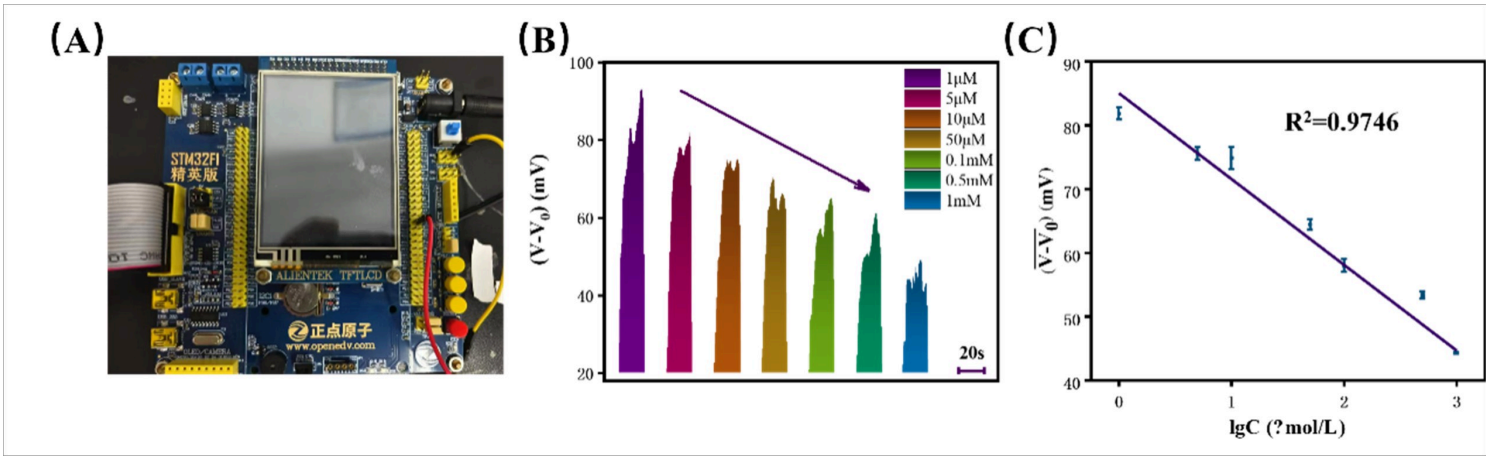


Figure 8

Portable PEC sensor: (A) Photocurrent responses of the device at different tetracycline concentrations (1, 5, 10, 50 μM; 0.1, 0.5, 1 mM). (B) Corresponding photocurrent response curves. (C) Linear calibration curve for tetracycline detection.

Supplementary Files

This is a list of supplementary files associated with this preprint. Click to download.

- TOC.png